Eddy Diffusivities for Heat in the Region near the Wall

By

Tokuro MIZUSHINA,* Ryuzo ITO*, Fumimaru OGINO*
and Hiroshi MURAMOTO*

(Received September 17, 1968)

The eddy diffusivities for heat were measured by the use of a Mach-Zehnder interferometer, and the ratio of eddy diffusivities for heat and momentum in the region close to the wall was predicted by a modified mixing length theory.

There was fairly good agreement between the experimental and theoretical results.

1. Introduction

The turbulent transport of heat between a flowing fluid which has a high value of Prandtl number and a wall is encountered in many engineering processes. Since the resistance for heat transfer is concentrated in the vicinity of the wall for high Prandtl number liquids, it is necessary to know the transfer machanism near the wall. In this region the turbulent transport of momentum and heat is governed not only by molecular motion but also by small eddy motion, but little is known about the behaviour of these small eddies, because of insufficient theoretical investigations and reliable experimental data.

Jenkins[1], Deissler[2], Azer and Chao[3] and Mizushina and Sasano[4] modified the mixing length theory in their analyses. However, the results obtained by these investigators are considerably different from each other and, since these were derived for the eddies in the turbulent core, do not represent the authors' data near the wall.

Measurements of temperature and concentration distributions in turbulent transfer have been made by several investigators[5],[6], but because of the inaccuracy of the data near the wall, more accurate experimental data are desirable.

This paper reports an analytical investigation for the ratio of the eddy diffusivities for heat and momentum and the experimental data of eddy diffusivities for heat near the wall.

The temperature distribution near the wall was measured precisely by means

* Department of Chemical Engineering.

of a Mach-Zehnder interferometer. The optical method is superior to the ordinary traversing method, since the former avoids disturbing the flow.

2. Mach-Zehnder Interferometer

A number of studies have been made on the precision and adjustment of a Mach-Zehnder interferometer, such as done by Hansen[7] and Schardin[8]. The Mach-Zehnder instruments have also been utilized by many investigators[9] in a comprehensive study of free convection and thermal boundary layers.

Figure 1 is a schematic diagram of the interferometer and associated optical equipments.

The light from source H, passing through an aperture S, is rendered parallel by the lens L_2 and is divided by the beam-splitter, plate 1. The transmitted beam A proceeds to the plane mirror 2 and the reflected beam B to the plane mirror 3. The two beams are recombined by the plate 4, and produce interference fringes which are focussed on the screen P by the lens L_3.

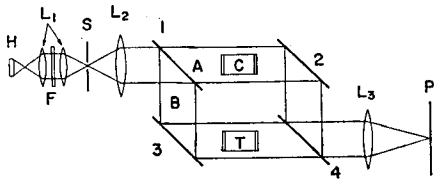

H	Light Source	L_3	Focusing Lens
L_1	Condenser Lens	P	Screen
F	Filter	A	Transmitted Beam
S	Slit	B	Reflected Beam
L_2	Collimating Lens	C	Compensating Cell
1,4	Splitter Plate	T	Test Section
2,3	Plane Mirror		

Fig. 1. Schematic Diagram of the Mach-Zehnder Interferometer and Associated Optical Apparatus.

In the authors' instrument, plates 1 and 4, plane mirrors 2 and 3 are circular, 100 mm in diameter. Aluminum coatings on the plates providing for half transmission and half reflection are made by evaporating aluminum metal in vacuum. The light source is a high pressure, 75 watt, Toshiba SHL-100UV type mercury arc lamp.

3. Experimental Apparatus and Procedure

The fluid flows in a rectangular duct; it is 10 mm high and 100 mm wide, and so the effects of the side walls may be neglected.

The test section, which is made of brass, is shown in Figure 2. The windows are high quality optically flat glass plates of uniform thickness (10 mm), thereby avoiding distortion of the interference fringes. The glass plates are mounted parallel to each other. The test section is placed in path B of the interferometer, as shown in Figure 1. In order to equalize the light beam path length, a com-

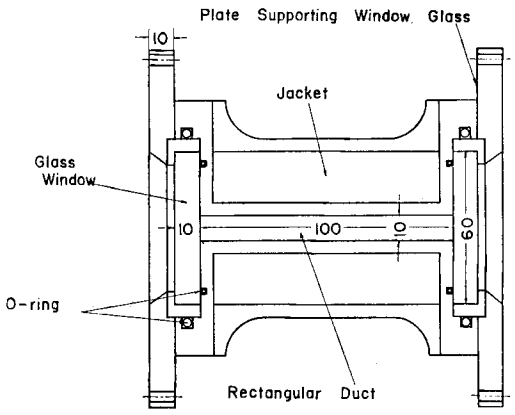

Fig. 2. Cross Section of Testing Duct.

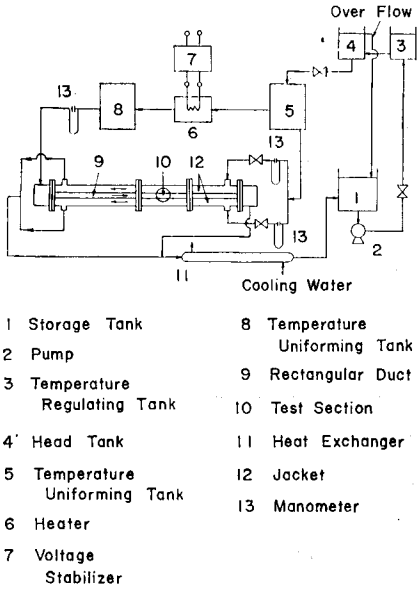

Fig. 3. Diagram of Flow System.

pensating chamber, whose width is the same as that of the test section and glass windows are similar to those of the test section in both thickness and quality, is placed in path A.

The rectangular ducts, one 220 cm long and the other 70 cm long, are made of brass, and both have the same inside dimensions as the test section. They are connected to the test section, the longer one at the upstream end and the shorter one at the downstream end, so as to make calming sections (Figure 3). The upstream length is $L/D_{eq}=120$; hence the flow in the test section may be considered to be thermally fully developed.

The fluid is circulated by means of a vinyl chloride pump through a 0.2 m^3 stainless steel storage tank. A head tank is used in order to provide a constant head for uniform flow, and the temperature regulating tank, in which a thermoregulator is provided, is used to keep the temperature of the fluid constant.

The fluid from the head tank is introduced into a stainless steel mixing tank, which is used in order to make the temperature of the fluid uniform, and it is divided into two flows. One flow is introduced directly into the jackets and the other, after being heated slightly by an electric heater, passes through a temperature uniforming tank and then enters the rectangular duct. The latter fluid is cooled by the colder fluid in the jackets. The fluids in the duct and jackets flow counter-currently.

In order to prevent the circulating fluid from contamination, vinyl chloride

plastic valves and pipes are used throughout the system. The flow rates are measured with calibrated orifices.

Before measuring the temperature distribution, the interferometer was first adjusted with the aid of a telescope to give fringes of proper width, perpendicular to the wall where heat transfer occurs. The fringes were focussed in a vertical plane just beyond the glass window at the side of plate 4 of the interferometer. Next, the temperature gradient was established by heating the fluid flowing in the duct. The telescope was then replaced by a camera. Kodak TRI-X Pan films with 10 to 20 seconds exposure were found satisfactory for this purpose. The negatives were magnified on a photographic plate. The over-all magnification was approximately 60 times. The fluids used were water and aqueous solutions of glycerol. The temperature of the fluid was kept at about 26～50°C, and the temperature difference between the fluid and the wall was about 0.01～0.3°C. Prandtl numbers and Reynolds numbers were varied through the ranges 6～40 and 10,000～24,000 respectively.

4. Method of Analyzing Interferograms

(1) Calculation of Temperature Profile from an Interferogram

The local changes of the temperature in the fluid, with the resultant changes in the refractive index, cause the displacement of interference fringes. The measurement of the displacement of the local fringes gives an accurate quantitative value of the local temperature at any point in the fluid.

If the refractive index of the fluid in the test section changes from n_∞ to n, the interference fringes are shifted and it follows

$$l(n-n_\infty) = m\lambda \tag{4.1}$$

where l the width of the liquid over which the light beam passes, m the number of fringe shifts, and λ the wave length of the light used respectively; the quantity m need not be an integer.

In the region in which temperature change is slight, a linear relationship may be assumed, that is,

$$n = n_\infty + \frac{dn}{dT}(T-T_\infty) \tag{4.2}$$

where T is the temperature of the fluid.

From equations (4.1) and (4.2), it follows that

$$T-T_\infty = \frac{m\lambda}{l\dfrac{dn}{dT}} \tag{4.3}$$

The flow in a rectangular duct may be assumed to be two-dimensional and if the temperature distribution exists in a transverse direction to flow direction, the interference fringes are shifted in the way shown in Figure 4 (b).

The x-, y-, and z-axis are assumed in the direction of the fluid flow, perpendicular to the horizontal wall, and in the direction of the light beam respectively (see Figure 4 (a)).

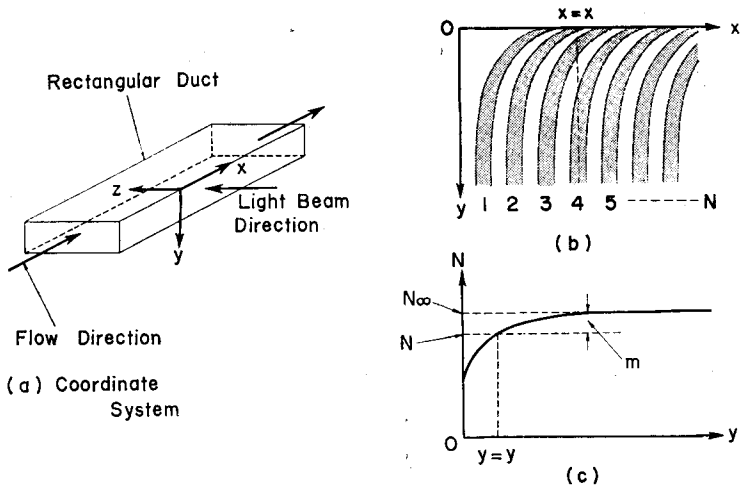

Fig. 4. Fringe Displacements and Plot of Fringe Displacements

Plotting the fringe number N in a fixed yz- plane against position y as abscissa gives a straight line which is parallel to the abscissa for the fringes with no refractive index disturbance in the interferometer. The plot deviates from a straight line in the disturbed part of the fluid, so that at each y value the fringe shift is given directly by the difference in the ordinates of the two curves (Figure 4 (c)), i.e. $m=N_\infty - N$, and the temperature distribution can be calculated by using equation (4.3).

(2) Refraction Effects

Refraction of the interferometer beam in passing through the region in which the temperature gradient exists, owing to the lens action of this region, cannot be avoided.

The incident light beam at $y=y_i$, parallel to the wall, refracts as shown in Figure 5 and produces virtual interference fringes at $z=l$.

If the refractive index n is assumed to be a function of y only, the following equation is obtained from Snell's law.

$$n(y_i) \sin \frac{\pi}{2} = n(y) \sin \varphi \tag{4.4}$$

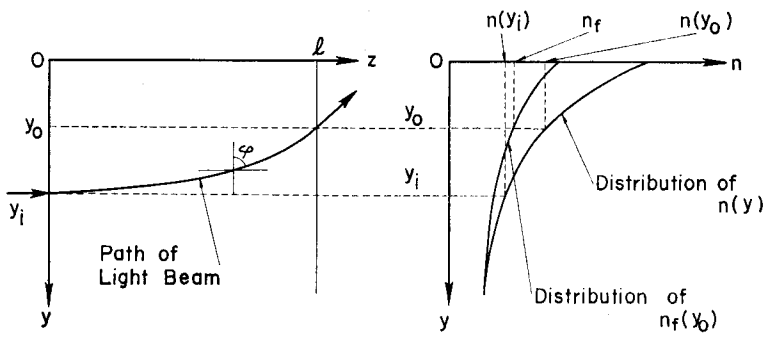

Fig. 5. Light Beam through a One-dimensional Refractive Index Field $n=n(y)$ and the Distribution of n and n_f.

The equation of the path of the light beam reads

$$\frac{dz}{dy} = -\tan\varphi \tag{4.5}$$

From equations (4.4) and (4.5), the following equation is obtained.

$$l = n(y_i)\int_{y_0}^{y_i} \frac{dy}{\sqrt{n(y)^2 - n(y_i)^2}} \tag{4.6}$$

This equation determines the relation between $n(y_i)$ and $n(y_0)$.

The average refractive index over the entire path length of the light beam reads

$$n_{av} = \frac{1}{l'}\int_{y_0}^{y_i} \frac{n(y)^2}{\sqrt{n(y)^2 - n(y_i)^2}}\, dy \tag{4.7}$$

where l' is the actual path length of the light beam and it follows

$$l' = \int_{y_0}^{y_i} \frac{n(y)}{\sqrt{n(y)^2 - n(y_i)^2}}\, dy \tag{4.8}$$

n_{av} is the refractive index obtained from an interferogram and given by using equation (4.1) as

$$n_{av}l' - n_\infty l = m\lambda \tag{4.9}$$

However, since l' is not known, l is used for the path length instead. Thus the refractive index obtained by using l is given by

$$n_f l - n_\infty l = m\lambda \tag{4.10}$$

From equations (4.7), (4.9), and (4.10) it follows

$$n_f = \frac{1}{l}\int_{y_0}^{y_i} \frac{n(y)^2}{\sqrt{n(y)^2 - n(y_i)^2}}dy \tag{4.11}$$

Since n_f is obtained by the interference at $z=l$, n_f is considered to be a function of y_0, i.e. $n_f=n_f(y_0)$. (see Figure 5)

Equation (4.11) determines the relation of n_f, $n(y_i)$ and $n(y_0)$, that is, $n_f(y_0) = n_f[n(y_i), n(y_0)]$. Eliminating $n(y_i)$ from the two equations (4.6) and (4.11), it follows

$$n_f(y_0) = n_f[n(y_0)] \tag{4.12}$$

Since $n_f(y_0)$ is obtained by equation (4.10), the functional form of $n(y)$ can be obtained by equation (4.12).

Computation was performed by assuming that $n(y)$ is approximated as a linear function of y in a small interval and the digital computer KDC-II of Kyoto University was used.

5. Analysis on the Ratio of the Eddy Diffusivities for Heat and Momentum

The basic concept is that the spherical eddy particle loses a part of its heat and momentum as it travels over a distance equal to the mixing length.

Assuming Newton's law for the drag force on an eddy particle, the following expressions are obtained.

$$\frac{\varepsilon_M}{\nu} = \eta_M \frac{lv}{\nu} \tag{5.1}$$

$$\eta_M = \frac{1}{\phi_M}\frac{\exp(2\phi_M)-1}{\exp(2\phi_M)+1} \tag{5.2}$$

$$\phi_M = \left(K\frac{l}{R}\frac{u}{v}\frac{1}{\eta_M}\right)^{1/2} \tag{5.3}$$

where l and R are the mixing length and the radius of the eddy particle respectively and K is a constant.

It may be reasonable to consider that $\partial u/\partial x \propto u/R$ and $\partial v/\partial y \propto v/l$. Thus, from the continuity equation,

$$\frac{l}{R} \propto \frac{v}{u} \tag{5.4}$$

Hence, one can obtain the result,

$$\eta_M = \text{constant} \tag{5.5}$$

On the other hand, an analysis closely similar to Mizushina and Sasano[4] on transport of heat by an eddy particle gives

$$\frac{\varepsilon_H}{\nu} = \eta_H \frac{lv}{\nu} \tag{5.6}$$

$$\eta_H = \phi_H\left\{1-\exp\left(-\frac{1}{\phi_H}\right)\right\} \tag{5.7}$$

$$\phi_H = \frac{Pr}{3}\frac{(R/l)^2\left(\frac{1}{\eta_M}\frac{\varepsilon_M}{\nu}\right)}{1+0.3\sqrt{2}\left(\frac{R}{l}\frac{1}{\eta_M}\frac{\varepsilon_M}{\nu}\right)^{1/2}Pr^{1/3}} \tag{5.8}$$

In the above expressions Ranz and Marshall's relation[10] is assumed on the heat transfer from an eddy particle to the surroundings.

The mixing length l and the radius R are assumed to depend on local flow conditions and the value of l is assumed to be determined by the value of R and the local Reynolds number Rv/ν.

Thus

$$\frac{l}{R} = f_n\left(\frac{Rv}{\nu}\right) \tag{5.9}$$

Since η_M is a constant,

$$\frac{l}{R} = F_n\left(\frac{\varepsilon_M}{\nu}\right) \tag{5.10}$$

The simplest form is

$$\frac{l}{R} = c\left(\frac{\varepsilon_M}{\nu}\right)^n \tag{5.11}$$

Since it may be assumed $u \approx v$ in the turbulent core, one obtains l/R=constant, that is, the power number n in equation (5.11) is zero. Hence, one can obtain the following equation in the turbulent core.

$$\phi_H = \frac{Pr}{3}\frac{(c_1^2/\eta_M)(\varepsilon_M/\nu)}{1+0.3\sqrt{2c_1/\eta_M}(\varepsilon_M/\nu)^{1/2}Pr^{1/3}} \tag{5.12}$$

In the vicinity of the wall u is proportional to the distance from the wall and v is proportional to the square of the distance, therefore one obtains

$$\frac{l}{R} = c\left(\frac{\varepsilon_M}{\nu}\right)^{1/3} \tag{5.13}$$

that is,

$$\phi_H = \frac{Pr}{3}\frac{(c_2^2/\eta_M)(\varepsilon_M/\nu)^{1/3}}{1+0.3\sqrt{2c_2/\eta_M}(\varepsilon_M/\nu)^{1/3}Pr^{1/3}} \tag{5.14}$$

As seen from equations (5.7) and (5.12), η_H approaches unity when ε_M/ν increases to infinity. From equations (5.1) and (5.6), the ratio of the eddy diffusivities is

$$\sigma = \frac{\varepsilon_H}{\varepsilon_M} = \frac{\eta_H}{\eta_M} \tag{5.15}$$

Since η_M is a constant,

$$\lim_{\varepsilon_M/\nu\to\infty}\sigma = \frac{1}{\eta_M} \tag{5.16}$$

From the authors' and Mizushina and Kuriwaki's[11] data for high Prandtl number, the value of lim σ is supposed to be unity and so the value of η_M is taken to be unity. Hence, the following expression is obtained.

$$\sigma = \phi_H\left\{1-\exp\left(-\frac{1}{\phi_H}\right)\right\} \tag{5.17}$$

The values of c_1 and c_2 in equations (5.12) and (5.14) were computed so as to fit the experimental data of ε_H/ν at $y^+=20$ by using assumed distribution of the eddy diffusivity for momentum as follows,

$$y^+>30 \qquad \frac{\varepsilon_M}{\nu} = 0.4\,y^+-1 \tag{5.18}$$

$$y^+\leqq 30 \qquad \frac{\varepsilon_M}{\nu} = 4.16\times10^{-4}\,y^{+3} \tag{5.19}$$

These assumed distributions are in fairly good agreement with the predictions of Wasan, Tien and Wilke[12].

Using the numerical values of c_1 and c_2, the equations (5.12) and (5.14) are rewritten as follows,

$$y^+>20 \qquad \phi_H = \frac{0.0166\left(\frac{\varepsilon_M}{\nu}\right)Pr}{1+0.200\left(\frac{\varepsilon_M}{\nu}\right)^{1/2}Pr^{1/3}} \tag{5.20}$$

$$y^+\leqq 20 \qquad \phi_H = \frac{0.0344\left(\frac{\varepsilon_M}{\nu}\right)^{1/3}Pr}{1+0.240\left(\frac{\varepsilon_M}{\nu}\right)^{1/3}Pr^{1/3}} \tag{5.21}$$

The results of this analysis are that σ is smaller than unity, that is, ε_H/ν is smaller than ε_M/ν, and ε_H/ν approaches to ε_M/ν when the values of Prandtl number and ε_M/ν increases to infinity.

6. Experimental Results

Typical temperature distribution which was corrected by taking into account the refraction effect is shown in Figure 6.

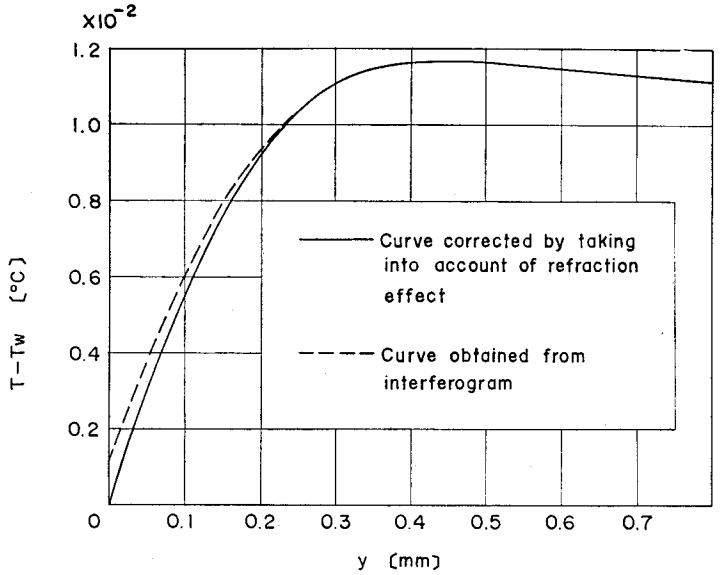

Fig. 6. Typical Temperature Distribution in Turbulent Flow of Viscous Liquid (Pr=39.5, Re=11,800)

The values of ε_H/ν were calculated from the temperature profiles. In this calculation the effects of the axial transport of heat by convection and the energy dissipation were taken into account. The temperature gradients in the x-direction, $\partial T/\partial x$, were calculated from the width of the interference fringes.

The turbulent energy dissipation function was assumed to be

$$\mu\phi^{(t)} = \rho\varepsilon_M\left(\frac{dU}{dy}\right)^2 \tag{6.1}$$

This assumption may be applied to the buffer region, but may not be applied to the region very close to the wall. However, in the region very close to the wall $\mu\phi^{(t)}$ is very small in comparison with $\mu\phi^{(l)}$, and so the assumption (6.1) may be appropriate even in that region.

The wall heat flux q_w was computed from the temperature gradient at the wall.

In Figure 7 the data of ε_H/ν from one of the experimental runs are shown with the plots of the equations of other investigators[5),13)] for ε_D/ν and ε_M/ν. The data of ε_H/ν are smaller than the values of ε_D/ν and ε_M/ν. However, equation (5.17) predicts both the values of ε_H/ν and ε_D/ν fairly well.*)

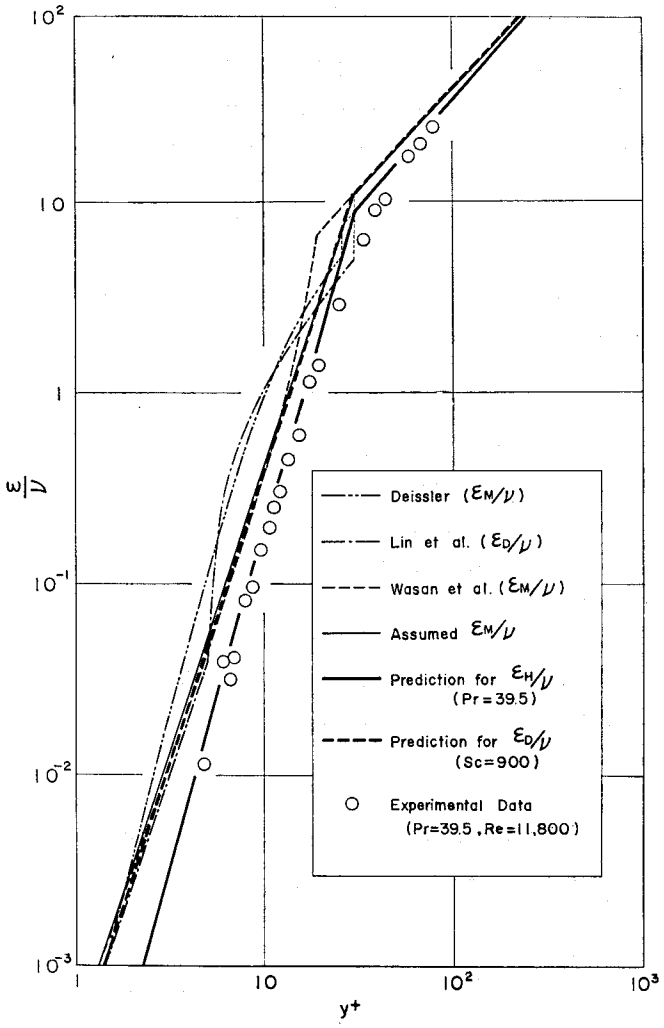

Fig. 7. Eddy Diffusivity Distribution.

* It was assumed that mechanisms for eddy diffusion for heat and mass are analogous.

7. Conclusions

The temperature profiles near the wall were measured by means of a Mach-Zehnder interferometer. The refraction effect of the light beam on the temperature profile was taken into account.

In the region close to the wall the values of ε_H/ν are smaller than the predictions of other investigators for ε_M/ν and the data of ε_D/ν by Lin, Moulton and Putnum[5].

On the other hand, the ratio of eddy diffusivities for heat and momentum was predicted by a modified mixing length theory. The predictions of the theory represent not only the data of ε_H/ν but also the values of ε_D/ν by Lin, Moulton and Putnum[5].

Acknowledgement

The authors wish to express their thanks to the Ministry of Education of Japan for financial support.

Nomenclature

c	:	A constant in equation (5.11)	[—]
c_1	:	A constant in equation (5.12)	[—]
c_2	:	A constant in equation (5.14)	[—]
D_{eq}	:	Equivalent diameter	[cm]
K	:	A constant in equation (5.3)	[—]
L	:	Length of upstream calming section	[cm]
l	:	Distance between glass windows or Mixing length	[cm]
l'	:	Path length of light beam	[cm]
m	:	Number of fringe shifts	[—]
N	:	Fringe number	[—]
N_∞	:	Fringe number at center of two parallel walls	[—]
n	:	Refractive index	[—]
n_{av}	:	Average refractive index	[—]
n_f	:	Refractive index obtained from interferogram	[—]
n_∞	:	Refractive index at center of two parallel walls	[—]
Pr	:	Prandtl number	[—]
q_w	:	Heat flux at wall	[cal/cm^2·sec]
R	:	Radius of eddy particle	[cm]
$Re=D_{eq}U/\nu$	:	Reynolds number	[—]
Sc	:	Schmidt number	[—]

T	:	Temperature of fluid	[°C]
U	:	Time-smoothed velocity in x-direction	[cm/sec]
u	:	Intensity of fluctuating velocity in x-direction	[cm/sec]
u_*	:	Friction velocity	[cm/sec]
v	:	Intensity of fluctuating velocity in y-direction	[cm/sec]
x	:	Rectangular coordinate	
y	:	Rectangular coordinate	
$y^+=yu_*/\nu$	:	Dimensionless distance from wall	[—]
y_i	:	Position of incident light beam	
y_0	:	Position of light beam at $z=l$	
z	:	Rectangular coordinate	
ε_D	:	Eddy diffusivity for mass	[cm^2/sec]
ε_H	:	Eddy diffusivity for heat	[cm^2/sec]
ε_M	:	Eddy diffusivity for momentum	[cm^2/sec]
η_H	:	Equation (5.7)	[—]
η_M	:	Equation (5.2)	[—]
λ	:	Wave length of light	[cm]
μ	:	Viscosity of fluid	[g/cm·sec]
ν	:	Kinematic viscosity of fluid	[cm^2/sec]
ρ	:	Density of fluid	[g/cm^3]
σ	:	Ratio of eddy diffusivities for heat and momentum	[—]
$\phi^{(l)}$	:	Laminar dissipation function	[1/sec^2]
$\phi^{(t)}$	:	Turbulent dissipation function	[1/sec^2]
ϕ_H	:	Equation (5.8)	[—]
ϕ_M	:	Equation (5.3)	[—]
φ	:	Angle of refraction	[—]

References

1) R. Jenkins; Heat Transfer and Fluid Mechanics Institute, Stanford Univ., 147 (1951).
2) R.G. Deissler; NACA Research Memorandum, E52F05, 1 (1952).
3) N.Z. Azer and B.T. Chao; Int. J. Heat and Mass Transfer, **1,** 121 (1960).
4) T. Mizushina and T. Sasano; International Developments in Heat Transfer, ASME, 662 (1961).
5) C.S. Lin, R.W. Moulton and G.L. Putnum; Ind. Eng. Chem., **45,** 636 (1953).
6) F. Jr. Page, W.G. Schlinger, D.K. Breaux and H. Sage; Ind. Eng. Chem., **44,** 424 (1952).
7) G. Hansen; Z. tekhn. Physik, **12,** 436 (1931).
8) H. Schardin; Z. Instrumentenk., **53,** 396, 424 (1933).
9) U. Grigull and H. Rottenkolber; J. Optical Soc. Am., **57,** No. 2, 149 (1967).
10) W.E. Ranz and W.R. Marshall; Chem. Eng. Progress, **48,** No. 3, 141 (1952).
11) T. Mizushina and Y. Kuriwaki; J. Engineering Physics, **12,** No. 2, 152 (1967).
12) D.T. Wasan, C.L. Tien and C.R. Wilke; A.I. Ch. E. Journal, **9,** 567 (1963).
13) R.G. Deissler; NACA Rep. 1210 (1955).